Extending the Coverage Area of Regional Ionosphere Maps Using a Support Vector Machine Algorithm

Mingyu Kim[1] and Jeongrae Kim[1]

[1]School of Aerospace and Mechanical Engineering, Korea Aerospace University, Goyang-si, 10540, Korea

Correspondence to: Jeongrae Kim (jrkim@kau.ac.kr)

Abstract. The coverage of regional ionosphere maps is determined by the distribution of ground monitoring stations, e.g. GNSS receivers. Since ionospheric delay has a high spatial correlation, ionosphere map coverage can be extended using spatial extrapolation methods. This paper proposes a support vector machine (SVM) to extrapolate the ionospheric map data with solar and geomagnetic parameters. One year of IGS ionospheric delay map data over South Korea is used to train the SVM algorithm. Subsequently, one month of ionospheric delay data outside the input data region is estimated. In addition to solar and geomagnetic environmental parameters, the ionospheric delay data from the inner data region are used to estimate the ionospheric delay data for the outside region. The accuracy evaluation is performed at three levels of range – 5˚, 10˚, and 15˚ outside the inner data regions. The estimation errors are 0.33 TECU for the 5˚ region and 1.95 TECU for the 15˚ region. These values are substantially lower than the GPS Klobuchar model error values. Comparison with another machine learning extrapolation method, the neural network, shows a substantial improvement of up to 26.7%.

1 Introduction

Ionospheric delay is one of the main error sources for single-frequency global navigation satellite system (GNSS) receivers. Ionosphere models or ionosphere maps can be used to correct for ionospheric delay. For real time applications, a regional ionospheric map using regional GNSS monitoring stations can be used to provide highly accurate corrections. The regional ionosphere map coverage is determined by the distribution of GNSS ground monitoring stations. Since ionospheric delay has a high spatial correlation, ionosphere map coverage may be extended by using spatial extrapolation methods. In addition to the spatial correlations, hourly/daily indices and solar/geomagnetic indices can serve as input parameters for the extrapolation.

A series of research studies have been conducted on the temporal extrapolation (prediction) of regional ionospheric maps using past observations. With respect to using machine learning algorithms, Kumluca et al. (1999) applied the neural network (NN) method to forecast ionospheric critical plasma frequencies, f_oF_2. McKinnell and Friedrich (2007) used an NN to predict the lower ionosphere in the aurora zone. Fokohlema et al. (2011a) performed a total electron content (TEC) prediction in South Africa using an NN based on solar and geomagnetic activity, time information, and user location information. Okoh et al. (2016) developed a regional VTEC model for Nigeria based on observational data from 12 stations and tested temporal and spatial extrapolation performance. Unlike previous studies, the extrapolation performance was improved by adding the International Reference Ionosphere (IRI) as an input. Razin and Voosoghi (2016) applied a wavelet NN with particle swarm optimization to predict the TEC over Iran. Huang and Yuan (2014) used time and temporal variation of the TEC values as radial-basis function (RBF) network inputs to temporal extrapolation.

On the other hand, research on the spatial extrapolation of the ionosphere map is sparse. Wielgosz et al. (2003) used kriging and multiquadric method to produce instantaneous TEC maps near the Ohio CORS stations in near-real time. Kim and Kim (2014) applied a biharmonic spline method to extend a small ionospheric correction coverage area. Ionospheric delay observations were used as the input parameters, and the TEC outside the coverage area was predicted. Leandro and Santos (2006) used geographical information as inputs of a NN model for spatial extrapolation of TEC over Brazil. For spatial extrapolation, Jayapal and Zain (2016) used a NN with time and solar/geomagnetic indices. Kim and Kim (2016) additionally used ionospheric delays in the inner ionospheric coverage area.

In addition to the NN method, a support vector machine (SVM) algorithm can be considered for spatial extrapolation. An SVM finds a solution to the convex quadratic programming problem in training to optimize the margin so that it can be both optimal and unique. On the other hand, an NN finds the weight between each layer through the gradient descent method, and the solution has a possibility to fall into the local minima in this process. An NN is based on empirical risk minimization (ERM), which is a method of minimizing learning errors during the learning process. On the other hand, an SVM is based on structural risk minimization (SRM), so it has excellent generalization performance (Gunn, 1998). SVMs have been widely used as predictive models in various fields. Huang et al. (2015) successfully performed stock market movement predictions using an SVM. Mohandes et al. (2014) performed wind speed predictions using an SVM and compared the performance against the NN method. The results showed that the SVM achieved superior prediction performance.

This paper proposes an SVM algorithm to extend ionosphere map coverage by applying temporal/environmental parameters and ionospheric observations. The IGS ionospheric map is used as a reference map, and the extrapolation accuracy of the SVM is evaluated by comparing it to the IGS map data. The extrapolation accuracies are compared with the GPS Klobuchar model and the NN model.

2 Parameter Modeling

Three types of input parameters are used for the extrapolation of a regional ionospheric map – temporal parameters, environmental parameters, and ionospheric delay observations. An extrapolated ionospheric delay, TEC_{ext}, may be represented as a function of these three parameters.

$$TEC_{ext} = f(x_t, x_e, x_{obs}), \tag{1}$$

where x_t and x_e are the time and the environmental parameters, respectively. x_{obs} is ionospheric delay observations in the inner region.

The TEC variation is correlated with the diurnal and seasonal time variation, and the ionospheric delay reaches its maximum around 14 hours local time (LT) and its minimum around 2 LT. Also, the TEC is high in spring and autumn, and low in summer and winter. In order to adopt these correlations, time parameters are included in the extrapolation model. The diurnal variation is represented by an hour number ($0 \sim 23$ LT), and the seasonal variation is represented by a day number ($0 \sim 365$). To represent the repeatability of these variations, the time parameters are modeled as sinusoidal functions.

$$x_t = [S_D \quad C_D \quad S_H \quad C_H] \tag{2}$$

where S_D and C_D are the sine and cosine, respectively, of the day number, and S_H and C_H are the sine and cosine, respectively, of the hour numbers. The periods used for the sinusoidal functions are set to 24 hours and 365.25 days for the diurnal and seasonal parameters, respectively. The ionosphere activity is also highly correlated with solar and geomagnetic activity. Three parameters are selected to reflect the space environment – the F10.7 index, geomagnetic index Kp, and sunspot number (SSN).

$$x_e = [F10.7 \quad Kp \quad SSN] \tag{3}$$

The ionospheric delays in the inner area are employed for the extrapolation in the outer area. Past inner-area ionospheric delays are used to train the machine learning algorithms, and current inner-area delays are used for the extrapolation. The observation data set for the N observation points is derived as follows.

$$x_{obs} = [TEC_{obs}^1 \quad TEC_{obs}^2 \quad \cdots \quad TEC_{obs}^N] \tag{4}$$

3 Extrapolation methods

3.1 Support vector machine (SVM)

The SVM method is a machine learning theory proposed by Vapnik in 1995. It uses an algorithm to find a

hyperplane that maximizes the margin (Gunn, 1998). It is used in data classification and regression problems, and SVMs used in regression are referred to as support vector regression (SVR). An SVM sets the regression function, $f(x)$, such that target y is in the following range.

$$f(x) = \hat{y}_{SVM} = w^T x + b \tag{5}$$

$$f(x) - \varepsilon \leq y \leq f(x) + \varepsilon, \qquad \varepsilon > 0 \tag{6}$$

where x is the input that contains $[x_t \quad x_e \quad x_{obs}]$. y is the target that represents the true TEC in the extrapolation region. ε is the allowable error level for y. In many practical cases, y is not in the range of $(f(x) - \varepsilon, f(x) + \varepsilon)$, and y is frequently adjusted to the range of $(f(x) - \xi, f(x) + \xi)$, where ξ is a slack variable. The optimal regression function is determined when the total magnitude of the slack variable, $\sum_i \xi_i$, is
10
minimized. Also, the distance between $f(x)$ and the support vector should be maximized. The distance between the SVM and $f(x)$ is called the margin, and the margin may also be minimized. Therefore, the optimal regression function minimizes $\|w\|$ and ξ to achieve the maximum margin (Gunn, 1998).

$$\min \frac{\|w\|^2}{2} + C \sum_{i=1}^{n} (\xi_i^- + \xi_i^+) \tag{7}$$

Subject to $\quad y - f(x_i) - \xi_i \leq \varepsilon, \qquad if \quad y - f(x_i) \geq \varepsilon$

15
$$y - f(x_i) + \xi_i \geq -\varepsilon, \qquad if \quad y - f(x_i) \leq -\varepsilon \tag{8}$$

In the above equation, the superscript – denotes a lower boundary and + denotes an upper boundary. The slack variable disappears while expanding equations. C is the penalty set by users. As the C value approaches zero, the weight for the slack variable decreases and the relative weight for $\|w\|^2$ increases. Therefore, the regression function that maximizes the margin can be calculated. This implies that the regression function
20
differs from y. As C increases, the weight for the slack variable sum increases rather than maximizing the margin magnitude. Therefore, a regression function is calculated in a form similar to y. Eq. (7) can be modified using a dual problem, as follows.

$$\arg \ \min_{\beta} \frac{1}{2} \beta^T K(x_i, x_j) \beta - f^T \beta, \qquad f = -y + \varepsilon \tag{9}$$

where β is $\alpha^- - \alpha^+$, and α is Lagrange multiplier. K is a kernel function that maps input data x to a higher
25
dimension. Kernel functions have several functions, including linear and polynomial functions. The most commonly used functions are Gaussian kernel functions (Cristianini, 2001).

$$K(x, y) = exp\left(-\frac{\|x-y\|^2}{2\sigma^2}\right) \tag{10}$$

After mapping x to feature space, one can determine the optimal β by using quadratic programming (QP). The optimal regression function can be computed by using the following equation (Gunn, 1998).

30
$$f(x) = w^T x + b = \sum_{i=1}^{N} \beta_i^* K(x_i, x_j) + \frac{1}{n} \sum_{i=1}^{N} \sum_{j=1}^{N} \{y_i - \beta_j^* K(x_i, x_j)\} \tag{11}$$
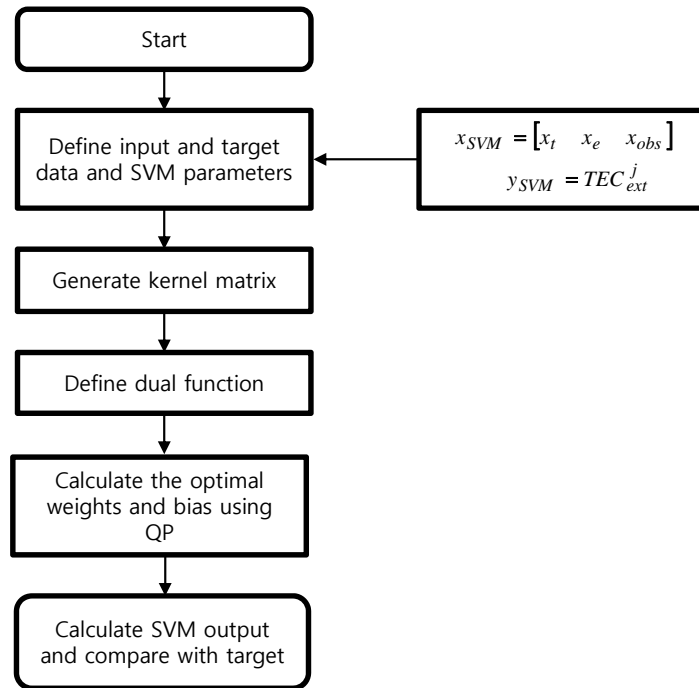
Figure 1: Flow chart of the SVM training process

The flow chart of the SVM training process is shown in Figure 1. The input variables consist of temporal
5 and environmental parameters and ionospheric delays in the observation region, and these inputs are identical
for each extrapolation point. Targets include the true TEC in the j-th extrapolation point. After the input/output
of the SVM is defined, a kernel matrix is generated for each input. Then, the training is performed to find the
optimal coefficients and bias of the regression function, $f(x)$. The kernel function is calculated for the epoch of
each input so that the size of the matrix becomes $N \times N$, where N is the number of epochs. As the input
10 increases, the computational time and memory usage also increase. Therefore, the elements of the kernel matrix,
including the oldest epoch, are deleted, and the kernel functions of the recent epoch are included in the matrix.
After defining the kernel function and the boundary of the regression function, the optimal weights and biases
are calculated using the interior point method. When the initial training is completed, the prediction and update
of the kernel function are repeated.

15

3.2 Neural network (NN)

An NN is a statistical learning model similar to a biological neural network. It consists of neurons or
perceptions, and a synapses. Neurons are interconnected with synapses, which store weights. An NN can solve
problems such as pattern recognition and regression by calculating the weights from the learning of the neurons
20 (Habarulema et al. 2011).

Several types of NNs exist – e.g. back-propagation neural network (BPNN), recurrent neural network
(RNN), and time delay neural network (TDNN). This study implements a BPNN, which is one of the most
commonly used NN algorithms. It is a feed-forward, multi-layer perceptron (MLP), supervised learning network
(Jwo et al, 2004). In the hidden layer, activation functions determine whether the values from the previous layer

are activated or not. Training is generally performed using gradient descent method.
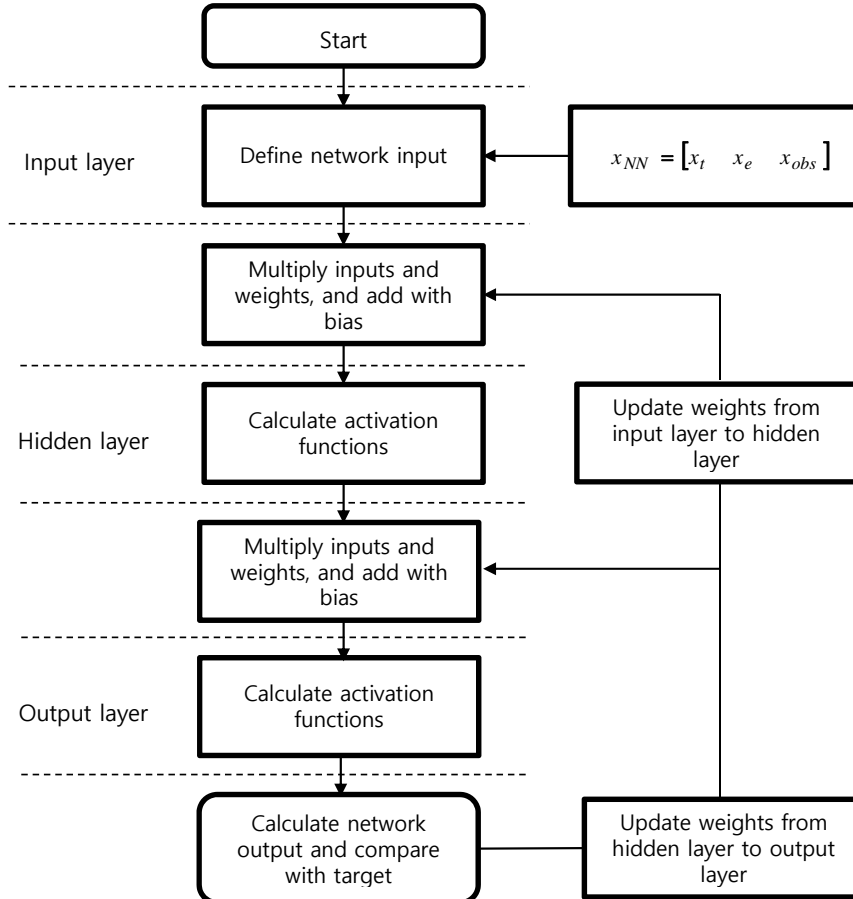
Figure 2: Flow chart of the neural network training process

Figure 2 shows a flow chart of the BPNN used for the regional ionospheric map extrapolation. The input layer includes the network inputs, x_{NN}, shown in Eqs. (2), (3), and (4). The network inputs and targets are the same as those used in the SVM. An input neuron multiplied by a weight can be computed through the hidden layer towards the output neuron, as follows.

$$\hat{y}_{NN} = f^n(W^{n,n-1}f^{n-1}(W^{n-1,n-2}f^{n-2}(\cdots f^1(W^{1,0}x + b^1)\cdots + b^{n-2}) + b^{n-1}) + b^n) \tag{12}$$

where b is the network bias, n represents the n-th layer, and $W^{n,n-1}$ is the weight from $n-1$ to the n-th layer. x is the network input, which includes the three input parameters for extrapolation, and $\hat{y}_{NN}$ is the network output. f is an activation function. The hyperbolic tangent sigmoid function is implemented, which is the most widely used method. The network is trained using the BPNN algorithm with true ionospheric delays and three

15   input parameter sets to find the optimal weights and biases.

The network data is generally divided into training, validation, and test sets. The training set is used to calculate and update the weights. The validation set is used to verify the training results. The test set is finally used to calculate the prediction error. This paper uses three data sets divided by 70%, 15%, and 15%, respectively. A detailed implementation of the NN can be found in Kim and Kim (2016).

4 Data Processing

An IGS global ionosphere map (GIM) is used to acquire reference ionospheric delay data because of its high accuracy and global coverage. Regional ionospheric delay time series are generated with the GIM data, and they are used to train the extrapolation algorithms. The predicted (extrapolated) ionospheric delays outside the 10   observation area are compared with the GIM data to evaluate the accuracy. The IGS GIM grid size is 2.5° x 5°, but other regional ionosphere maps such as the SBAS ionosphere corrections have an equal latitude-longitude grid size. Therefore, a 5° x 5° grid size is used for the regional ionosphere map in this research. The IGS GIM provides the data with two-hour intervals.

Figure 3 illustrates the observation and extrapolation grid points. The observation regions (blue) are set 15   with a radius of 2,650 km centered on South Korea, and the extrapolation regions (red) are set with a radius of 4,500 km in order to include the 15° extended grid point from South Korea. Therefore, the latitude of the observation area ranges from 15°N to 55°N, and the longitude ranges from 105°E to 150°E. The accuracy evaluation points are selected to perform the extrapolation. In order to accommodate the directional characteristics of the extrapolation performance, the evaluation point set is selected for each direction (north, 20   south, east, and west). In each direction, three points are selected with different distances from the inner observation region – 5°, 10°, and 15°.
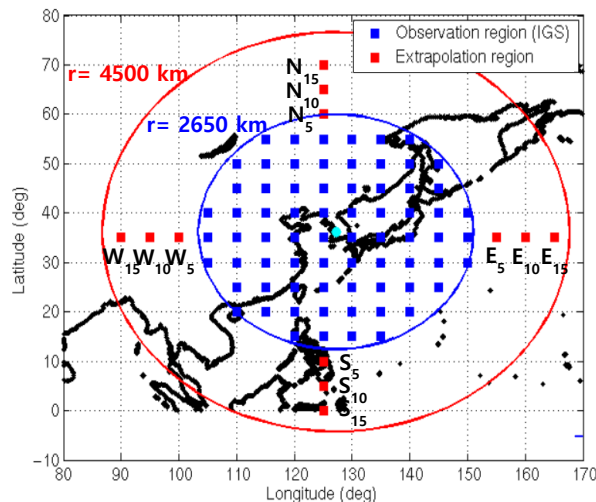
Figure 3: Observation and extrapolation regions of ionospheric delay grids

25

In the case with the environmental parameters (i.e. F10.7, Kp, and SSN), real-time data may not exist at the prediction epoch due to data latency. In order to simulate this data latency, previous one-epoch values are used instead of the current values during the extrapolation process. True environmental parameters are used in the training process, but the previous one-epoch values are used in the extrapolation process. The correlation

analysis between the current and previous one-epoch values confirms the correlation. The correlation coefficients between the two adjacent epochs of data for F10.7, Kp, and SSN are 0.930, 0.863, and 0.852, respectively. Since the IGS GIM uses 2-hour intervals, the Kp, which is provided every 3 hours, is interpolated at intervals of 2 hours.

5  Previous research showed that extrapolation errors have a high correlation with the ionospheric delay magnitude (Kim and Kim, 2014a). Therefore, the high ionospheric delay season is more appropriate when evaluating the extrapolation algorithm than the low ionospheric delay season. The training period is set to one year from October 1, 2013 to September 30, 2014. In this period, the minimum and maximum TEC are 5.1 and 112.2 TECU, respectively, as shown in Figure 4. The prediction period is set to one month from October 1 to 31,
10  2014.
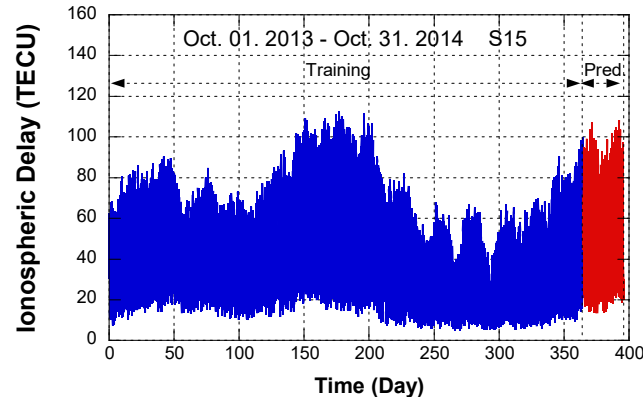
Figure 4: One year variation of ionospheric delay (October 01, 2013 to October 30, 2014, S15)

15  The training and prediction performance depend on user parameters. In the case of the NN, prediction performance mainly depends on the number of hidden neurons. If the number of hidden neurons is too high, over-fitting may occur, and the calculation time is long. Since there are no criteria for determining the number of hidden neurons, the optimal number of hidden neurons must be found by analyzing the prediction error variation due to the number of neurons. The number of hidden neurons is set to 80 based on previous studies
20  (Kim and Kim 2016). In the case of the SVM, the prediction result also varies with the model parameters. This paper sets the penalty, C, as 10^6, which causes the regression function to almost equal y. The Gaussian function, which is widely used in SVMs, is used as a kernel function, and σ is set to 10^{-6}. The values of σ and ε are selected via trial and error to determine the lowest prediction error case. They are set to 10^{-6} and 10^{-7}, respectively.

25 **5 Results**

  The regional ionosphere map extrapolation is performed using the SVM, and the IGS GIM is used as a truth value. The SVM extrapolation results are compared with the NN and Klobuchar model results. Hourly variations of the extrapolation results are analyzed with one-day data, and then daily variations of the results are analyzed with one-month data.

30 **5.1 Single-day extrapolation analysis**

  The variations of the TEC and the extrapolation results are analyzed for the data from October 28, 2014,

when the daily ionospheric delay magnitude reaches its maximum for the prediction period (October 2014).
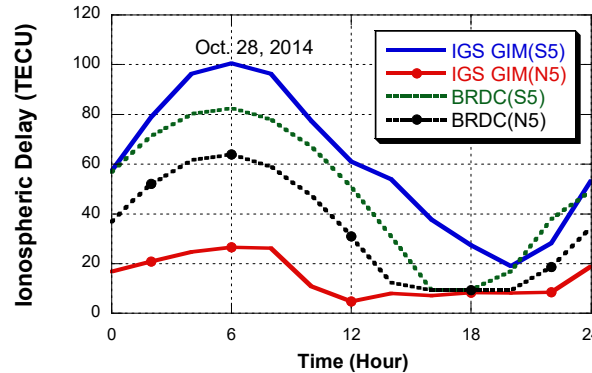
Figure 5: Ionospheric delays of the IGS GIM and Klobuchar model (south 5° and north 5° points)

Figure 5 shows the ionospheric delay variations of the IGS GIM and Klobuchar model on October 28, 2014. Data from two evaluation points, 5° north (N5, 60°N, 125°E) and 5° south (S5, 10°N, 125°E) are presented. Universal time (UT) is used. The ionospheric delay reaches its maximum at 15:00 LT (6:00 UT) and then decreases. There are large differences between the ionospheric delays at the north and south points because of the ionospheric spatial gradient (Kim et al. 2014). The north-south difference produced by the Klobuchar model TEC is significantly smaller than the IGS GIM TEC.
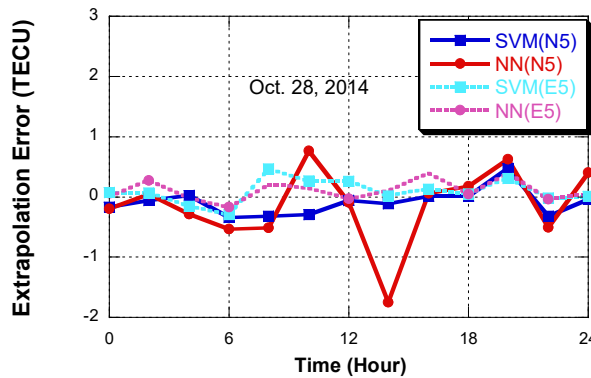
Figure 6: Extrapolation error variations on October 28, 2014 (north 5° and east 5° points)

15

Figure 6 shows the extrapolation results for October, 28, 2014. Two extrapolation points, north 5° (N5) and east 5° (E5), are selected. In the case of N5, the extrapolation RMS errors of the SVM and NN are 0.23 TECU and 0.63 TECU, respectively. The SVM outperforms the NN with a 63.5% error reduction. The difference in

error levels mainly results from the large NN error for N5 at 14:00 UT. The NN frequently shows some sort of divergence and causes a large error increase, but the SVM exhibits a smaller divergence problem. The SVM-NN difference at the east 5° (E5) point is not as significant as it is at the north 5° (N5) point, although the TEC magnitude is generally greater at the east point than at the north point due to its lower latitude.
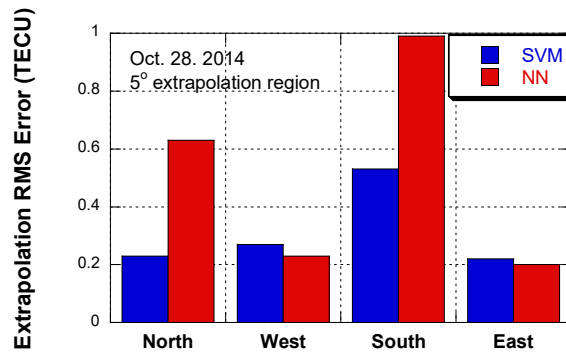
Figure 7: Extrapolation errors for each direction (5° extrapolation regions)

10   Figure 7 compares the RMS errors of four 5° extrapolation points (N5, S5, E5, and W5) on October 28, 2014. The error magnitude is the largest at the south point where the ionospheric delay magnitude is the largest. The SVM shows similar error levels for the north, east, and west points. However, the NN shows larger errors than the SVM even at the north point. This difference in extrapolation accuracy may be explained via the ionospheric spatial gradient. The spatial gradient along the north-south direction is significantly greater than the gradient along the east-west direction (Kim et al. 2014). The large gradient increases the geographical
15   ionospheric delay difference and frequently causes the NN error increase. However, the SVM is more robust for this large amount of gradient data.
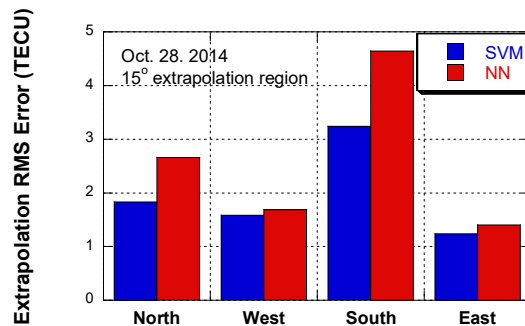
Figure 8: Extrapolation errors for each direction (15° extrapolation regions)

20

Figure 8 compares the RMS errors of four 15° extrapolation points (N15, S15, E15, and W15). The overall error level increases from that of the 5° points, but the SVM still outperforms the NN, particularly at the south and north points. The SVM error at the south point is 3.24 TECU, and the error reduction over the NN is 1.40 TECU, or 30.2%.

5   **5.2 One-month extrapolation analysis**

The spatial extrapolations are performed for the one-month period from October 1 to 31, 2014. As with the single-day extrapolation, the one-year data from October 2013 to September 2014 is used for the training process.
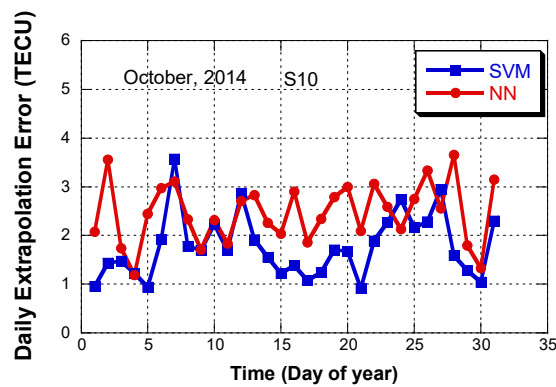
Figure 9: Daily extrapolation RMS error variations in October 2014 (south 10° point)

Figure 9 shows the daily extrapolation errors for the south 10° extrapolation point (S10) in October 2014. The one-month means of the daily RMS errors are 1.89 TECU for the SVM and 2.54 TECU for the NN. During 15   the 31 days, the SVM achieved better performance than the NN for 26 days (83.9%). During low ionospheric delay periods, the difference in extrapolation performance between the two methods is not significant (e.g. October 11 and 12). However, during high ionospheric delay periods, the difference becomes significant (e.g. October 28).
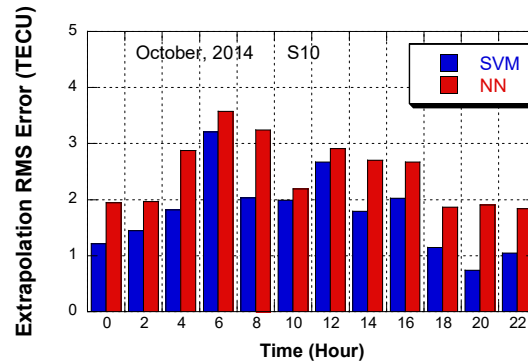
Figure 10: Extrapolation RMS errors for each two-hour interval on October 2014 (south 10° point)

In order to analyze the hourly extrapolation performance, the one-month mean of each two-hour time interval is presented in Figure 10. The time unit is UT. Both the SVM and NN show an increase in extrapolation errors at 06:00 UT. During the high TEC period, 04:00-08:00 UT, the mean of the SVM error is 0.88 TECU lower than the error of the NN. Even during the low TEC period, 18:00-22:00 UT, the SVM error is 0.88 TECU lower than the NN. These results prove that the prediction performance of the SVM model is better for both large and small ionospheric delays. A correlation analysis with the geomagnetic index, Kp, is performed by computing statistics for each Kp value. (This is not shown as a figure.) Over all Kp values, the SVM outperforms the NN with the same level of improvement. The only exception is Kp= 5 on October 5 12:00 UT, where the NN outperforms the SVM. However, this high Kp happens only one time among 360 epochs, and a generalized conclusion requires a further research.

Table 1: One-month mean of extrapolation RMS errors using the SVM, NN, and Klobuchar models (unit= TECU)

Extrapolation region	5°			10°			15°		
	BRDC	SVM	NN	BRDC	SVM	NN	BRDC	SVM	NN
North	14.41	0.32	0.68	13.07	1.02	1.06	12.04	1.97	1.90
East	14.63	0.17	0.20	14.57	0.51	0.71	14.47	1.00	1.13
West	13.38	0.24	0.25	13.29	0.64	0.63	13.12	1.27	1.44
South	25.13	0.57	0.67	24.40	1.89	2.54	26.97	3.58	3.79
Total	16.89	0.33	0.45	16.33	1.01	1.23	16.65	1.95	2.06

Table 1 summarizes the extrapolation errors for all evaluation points in October 2014. The one-month mean of the errors from four directions, north, south, east, and west, and three ranges, 5°, 10°, and 15°, are presented. The Klobuchar model of the GPS navigation message (BRDC) is also shown for comparison. In all ranges, even at the 15° points, both the SVM and NN outperform the Klobuchar model. This proves that the extrapolation methods are useful even in large areas. In the east and west points where the ionospheric spatial gradient is small, the accuracy improvement provided by the SVM is not significant, but the improvement increases as the distance of the extrapolation region increases. The SVM error is 11.8% smaller than that of the NN in the W15 region. In the south region, the extrapolation error is very large due to the large TEC magnitude variation, and these results in the largest improvement provided by the SVM. In particular, the S10 region contains the largest error difference at approximately 0.65 TECU. The average error for each region is the largest at the 10° extrapolation region. The difference may mainly result from the fact that the NN yields a local minimum instead of global minimum, and then the NN yields a large error.

6   Conclusions

The coverage area of a regional ionosphere map is determined by the distribution of GNSS ground stations. This paper proposes a spatial extrapolation algorithm to extend the ionosphere map coverage using an SVM. One year of IGS GIM ionospheric delay data over South Korea and environmental parameters are used as input
5   data sets to train the SVM algorithm. From the training results, one month of ionospheric delay data outside the input data region is estimated. In addition to solar and geomagnetic environmental parameters, current ionospheric delay data in the inner data region are used to estimate the ionospheric delay data in the outside region.

The estimation accuracy is evaluated at 12 points; four directions (north, south, east, and west) and three
10   distances (5˚, 10˚, and 15˚). The accuracy improvement by the SVM is compared with the NN. The one-month mean of the estimation error produced by the SVM is 0.33 TECU for the 5˚ region, 1.01 TECU for the 10˚ region, and 1.95 TECU for the 15˚ region. The improvement levels over the NN for the 5˚, 10˚, and 15˚ regions are 26.7%, 17.9%, and 5.3%, respectively. The NN estimation results frequently go into local minima instead of global minima, but the SVM results avoid this problem. The estimation error depends on the ionospheric delay
15   level and ionospheric spatial gradient. Among the four directions, the error in the south region is the largest, and the error in the north region is the second largest. The ionospheric delay in the north region is usually smaller than the delay either in the east or west, but the estimation accuracy in the north region is even larger than in the east or west. A larger spatial gradient along the south-north direction over the east-west direction may explain this difference.

20

Competing interests: The authors declare that they have no conflict of interest.

Acknowledgements. This research was supported by the Space Core Technology Development Program funded by the Ministry of Science and Information and Communications Technology (ICT) (NRF-
25   2016M1A3A3A02016943).

References

Cristianini, N.: Support vector and kernel machines. Tutorial at the 18th Int. Conf. Mach. Learn., 2001.

Gunn, S. R.: Support vector machines for classification and regression. ISIS Technical Report, 14, 1998.

30   Habarulema, J. B., McKinnell, L. A., Opperman, B. D. L.: Regional GPS TEC modeling; Attempted spatial and temporal extrapolation of TEC using neural networks. J. Geophys. Res., 116, 1-14, doi:10.1029/2010JA016269, 2011

Huang, W., Nakamori, Y., and Wang, S. Y.: Forecasting stock market movement direction with support vector machine. Comput. Operat. Res., 32, 2513-2522, doi:10.1016/j.cor.2004.03.016, 2015.

35   Huang, Z., and Yuan, H.: Ionospheric single-station TEC short-term forecast using RBF neural network. Rad. Sci., 49, 283-292, doi:10.1002/2013RS005247, 2014.

Jayapal, V., and Zain, A. F. M.: Interpolation and extrapolation techniques based neural network in estimating the missing ionospheric TEC data. In: Progress in Electromagnetic Research Symposium (PIERS), 695-699, 2016.

40   Jwo, D. J., Lee, T. S., Tseng, Y. W.: ARMA neural networks for prediction DGPS pseudorange correction. J. Navi., 57, 275-286, doi:10.1017/S0373463304002656, 2004.

Kim, J., Kim, M.: Extending ionospheric correction coverage area by using extrapolation methods. J. Kor. Soci. Aeros. Sci. Fli. Operat., 22, 74-81, doi:10.12985/ksaa.2014.22.3.074, 2014a.

Kim, J., Lee, S. W., Lee, H. K.: An annual variation analysis of the ionospheric spatial gradient over a regional area for GNSS applications. Adv. Spa. Res., 54, 333-341, doi:10.1016/j.asr.2014.03.024, 2014b.

5   Kim, M., Kim, J.: Extending Ionospheric Correction Coverage Area By Using A Neural Network Method. Int. J. Aero. Spa. Sci., 17, 64-72, doi:10.5139/IJASS.2016.17.1.64, 2016.

Kumluca, A., Tulunay, E., Topalli, I.: Temporal and spatial forecasting of ionospheric critical frequency using neural networks. Rad. Sci., 34, 1497-1506, doi:10.1029/1999RS900070, 1999.

Leandro, R. F. and Santos, M. C.: A neural network approach for regional vertical total electron content
10   modelling. Stud. Geophys. Geod., 51, 279-292, doi:10.1007/s11200-007-0015-6, 2006.

McKinnella, L. A., Friedrich, M.: A neural network-based ionospheric model for the auroral zone. J. Atmos. Sol. Terr. Phys., 69, 1459–1470, doi:10.1016/j.jastp.2007.05.003, 2007.

Mohandes, M. A., Halawani, T. O., Rehman, S., Hussain, A.: Support vector machines for wind speed prediction. Renewable Ener., 29, 939-947, doi:10.1016/j.renene.2003.11.009, 2014.

15   Okoh, D., Owolabi, O., Ekechukwu, C., Folarin, O., Arhiwo, G., Agbo, J., Bolaji, S., Rabiu, B.: A regional GNSS-VTEC model over Nigeria using neural networks: A novel approach. Geode. Geodyn., 7, 19-31, doi:10.1016/j.geog.2016.03.003, 2016.

Razin, M. R. G. and Voosoghi, B.: Wavelet neural networks using particle swarm optimization training in modeling regional ionospheric total electron content. J. Atmos. So. Terr. Phys. 149, 21-30,
20   doi:10.1016/j.jastp.2016.09.005, 2016.

Wielgosz, P., Grejner-Brzezinska, D., and Kashani, I.: Regional ionosphere mapping with kriging and multiquadric methods. J. GPS, 2, 48-55, doi:10.5081/jgps.2.1.48, 2003.